

THE ASTROPHYSICAL JOURNAL, 205:384-396, 1976 April 15
 © 1976. The American Astronomical Society. All rights reserved. Printed in U.S.A.

OH-IR STARS. II. A MODEL FOR THE 1612 MHz MASERS*

MOSHE ELITZUR, PETER GOLDREICH, AND NICK SCOVILLE*

California Institute of Technology

Received 1974 September 30; revised 1975 June 16

ABSTRACT

A model is presented for the 1612 MHz OH masers associated with infrared stars. Its principal conclusions are as follows. The central stars are losing $\sim 3 \times 10^{-5} M_{\odot} \text{ yr}^{-1}$, and the masers operate in the outer regions ($r > 10^{16} \text{ cm}$) of the circumstellar envelopes. The maser radiation is narrowly beamed in the radial direction, both inward and outward. Thus the two maser emission features originate in the near and the far sides of the expanding circumstellar gas. The 1612 MHz maser is powered by the absorption of 35μ photons which excite the OH molecules from the $^2\Pi_{3/2}, J = 3/2$ ground state to the $^2\Pi_{1/2}, J = 5/2$ state. The excited OH molecules return to the ground state by a series of radiative decays. In most cases, the radiative cascade proceeds directly down the $^2\Pi_{1/2}$ ladder. The final and the most important step in the pump cycle is the radiative decay from the $^2\Pi_{1/2}, J = 1/2$ state to the $^2\Pi_{3/2}, J = 3/2$ state. If the transitions which link these two states are optically thick, a strong inversion of the $F = 1 \rightarrow F = 2$ 1612 MHz transition is produced.

Subject headings: infrared: sources — masers — stars: circumstellar shells

I. INTRODUCTION

Shklovsky (1966) first suggested that OH masers might be pumped by the absorption of infrared radiation. Subsequently, the physics of the pump process was investigated by Litvak (1969) and by Litvak and Dickenson (1972). The present paper attempts to bring into sharper focus the essential features responsible for the inversion of the 1612 MHz transition in OH-IR stars. Although a short comparison of the current paper with earlier papers is presented in § Vd, the reader is urged to consult the earlier works for more details concerning their contents.

The plan of this paper is as follows. A discussion of the principal observational facts is contained in § II. Then a brief description of the gas kinematics and the OH abundance in the circumstellar envelopes about OH-IR stars is given in § III. Section IV is devoted to a detailed description of the population flow in the maser pump cycle and includes the results of numerical solutions of the equations of radiative transfer and statistical equilibrium. Finally, § V contains a comparison of the theoretical results and the observational facts.

II. PHENOMENOLOGICAL PICTURE

A model for the 1612 MHz OH masers associated with infrared stars should account for the main observational facts which are the following (Wilson and Barrett 1972):

1. The 1612 MHz emission is concentrated in two narrow velocity ranges separated by $20-50 \text{ km s}^{-1}$. The two emission features tend to have abrupt outer edges and more gradually tapering inner edges.

* Contribution No. 2542 of the California Institute of Technology, Division of Geological and Planetary Sciences.

2. The intensities of the two emission peaks are generally unequal, but statistically there is no tendency for either the high- or the low-velocity peak to be the stronger.

3. The brightness temperature of the 1612 MHz radiation is high, $T_B \approx 10^{10} \text{ K}$.

4. The masers are associated with late M-type Mira variables and supergiants. These are cool ($T_e \approx 2000 \text{ K}$), high-luminosity ($L \geq 10^4 L_{\odot}$), oxygen-rich ($[\text{O}]/[\text{C}] > 1$) stars.

5. The central stars are surrounded by circumstellar dust shells which absorb an appreciable fraction of the stellar radiation and reemit it at infrared wavelengths longward of 3μ (Hyland *et al.* 1972). The extent of the infrared emission region of one Mira variable, IRC +10011, has been measured at 2.2, 10, and 20μ by means of a lunar occultation (Zappala *et al.* 1974). At 10μ the bulk of the flux is emitted by the circumstellar dust shell which has an angular diameter of $0.^{\circ}135$ and a temperature of $\sim 600 \text{ K}$. Indirect arguments based on photometry suggest that the 20μ flux comes from a much larger region of $\sim 1''$ angular diameter. At the distance to IRC +10011 of $\sim 500 \text{ pc}$, $1''$ corresponds to a linear diameter of $\sim 7.5 \times 10^{15} \text{ cm}$.

6. The location of the maser sources with respect to the central stars is unknown. However, VLBI observations by Masheder, Booth, and Davies (1974) have shown that the 1612 MHz masers associated with the supergiants NML Cyg, VY Cma, and VX Sgr are grouped in clusters with dimensions of a few arcseconds. Furthermore, Reid and Muhleman (1975) have found that the angular spot sizes of the emission features associated with Mira variables are larger than $0.^{\circ}1$.

7. The intensities of the 1612 MHz OH masers associated with Mira variables vary in phase with the

intensity variations of the central stars (Harvey *et al.* 1974).

III. CIRCUMSTELLAR ENVELOPE

In Paper I (Goldreich and Scoville 1975), a detailed model of the circumstellar envelope of an OH-IR star is developed. The model parameters chosen in Paper I and all results obtained there are adopted in the present paper.

a) Kinematics

It is believed that most, if not all, of the central stars in OH-IR sources are evolved rather than newly born stars. The presence of circumstellar dust around these evolved stars implies that they are losing mass. It is assumed in this paper that the outflow velocity is just one-half of the velocity difference between the two OH emission features. The basis for this assumption is that in a constant velocity radial outflow, the line of sight velocity is constant only in the radial direction. Thus it seems likely that the longest maser gain paths are aligned in the radial direction and consequently that the maser radiation is beamed in the radial direction—both inward and outward. The two intensity peaks would then correspond to emission from the front and back of the expanding flow. This interpretation is supported by the details of the maser pump mechanism which is advocated in this paper. However, it disagrees with the traditional view which is that the higher OH velocity coincides with the stellar velocity and the lower OH velocity coincides with the velocity of the near side of the outflowing gas (Woolf 1972). Reid (1975) has critically analyzed the statistics of the velocities of the optical emission and absorption lines on which the traditional view is based. He shows that the velocities of the optical lines in Miras which are OH emitters have different statistical properties than those from the bulk of the Mira variables. He concludes that the statistical evidence does not support the traditional interpretation of the OH velocities. Kwok, Gilman, and Woolf (1974) have independently concluded that the velocities of the OH emission peaks correspond to the gas velocity in the front and back of the outflow from the central star. They suggest that the optical lines are redshifted due to scattering by dust grains imbedded in the escaping gas. In their opinion, the traditional view concerning the velocities of the OH emission peaks arose because these redshifts were not taken into account in the comparison of the optical line velocities and the OH maser line velocities.

The mechanism responsible for the ejection of gas from the central stars has not been convincingly identified. The most plausible candidates seem to be the direct acceleration of the gas by shock waves and the indirect acceleration by radiation pressure acting on dust grains imbedded in the gas. The VLBI observations and the pump model proposed in this paper indicate that the maser emission region is located at a distance $r \geq 10^{16}$ cm from the central star. Any residual acceleration of the gas at such a great distance from the central star can probably only

be produced by radiation pressure acting on the dust grains. For the model developed in Paper I, radiation pressure greatly exceeds gravity far from the star, and the equation of motion for the gas is

$$m_{\text{H}_2} n_{\text{H}_2} (1 + f/2) \frac{dv}{dr} = Q n_d \sigma_d \frac{L}{4\pi r^2 c}, \quad (1)$$

where $v(r)$ is the outflow velocity, $m_{\text{H}_2} n_{\text{H}_2} (1 + f/2)$ is the mass density, $f = n_{\text{H}}/n_{\text{H}_2}$, L is the stellar luminosity, and

$$Q n_d \sigma_d = \frac{-d\tau(r)}{dr}, \quad (2)$$

with $\tau(r)$ the optical depth to the stellar continuum from r to ∞ . Since f and $n_d(r)/n_{\text{H}_2}(r)$ are not expected to change beyond $r = 10^{16}$ cm, equation (1) may be integrated and yields

$$v^2 + \frac{Q n_d \sigma_d L}{2\pi m_{\text{H}_2} n_{\text{H}_2} (1 + f/2) c r} = v_\infty^2, \quad (3)$$

where $v_\infty \equiv v(r = \infty)$. For $r \geq 10^{16}$ cm, $(v_\infty - v)/v_\infty \ll 1$, and equation (3) may be rewritten in the form

$$v_\infty - v(r) = \tau(r) \frac{L}{c \Phi}, \quad (4)$$

where

$$\Phi \equiv 4\pi r^2 m_{\text{H}_2} n_{\text{H}_2} (1 + f/2) v \quad (5)$$

is the rate of mass loss.

A plausible set of parameters for OH-IR stars is $L = 10^4 L_\odot = 4 \times 10^{37}$ ergs s $^{-1}$, $\Phi \approx 3 \times 10^{-5} M_\odot \text{ yr}^{-1}$, $\tau(r = 10^{16} \text{ cm}) \approx 0.07$, and $v_\infty = 10^6 \text{ cm s}^{-1}$. These values imply

$$v_\infty - v(r) \approx \frac{0.47}{r_{16}} \text{ km s}^{-1}, \quad (6)$$

where $r_{16} \equiv r/(10^{16} \text{ cm})$.

b) OH Abundance

A detailed model of the circumstellar OH abundance was developed in Paper I (Goldreich and Scoville 1975). It was shown there that the OH abundance is controlled by chemical exchange reactions and by the dissociation of H₂O molecules. In the warm ($T \gtrsim 5 \times 10^2 \text{ K}$), inner ($r \lesssim 2 \times 10^{15} \text{ cm}$) region of the circumstellar envelope, the reaction OH + H₂ \leftrightarrow H₂O + H rapidly converts OH molecules into H₂O molecules. Beyond $2 \times 10^{15} \text{ cm}$, the gas kinetic temperature is so low ($T \lesssim 5 \times 10^2 \text{ K}$) that the exchange reaction is very slow and the mean lifetime of an OH molecule is greater than the expansion time for the circumstellar gas. In the outer region of the circumstellar envelope, OH molecules are produced from the photodissociation of H₂O molecules by interstellar ultraviolet radiation and from the dissociation

of H_2O molecules by collisions with dust grains. The predicted OH number density is greater than 1 cm^{-3} at $r \geq 10^{16} \text{ cm}$. In the present paper, the calculated OH abundance from Paper I is used as a guide in choosing appropriate values of n_{OH} for the numerical modeling of the pump mechanism.

IV. THE MASER

a) General Remarks

Based on the model developed in Paper I for the OH distribution in circumstellar envelopes about OH-IR stars, it is possible to make considerable progress toward understanding the pump mechanism for the 1612 MHz OH masers.

The correlated variations of the infrared and maser intensities rule out collisional pumps. Stellar luminosity variations can affect a collisional pump by changing the temperature of the colliding particles (mostly H_2 molecules and H atoms). However, the stellar radiation only couples indirectly to the H_2 molecules and H atoms by their collisions with the dust grains that stream through the gas. It is shown in § VI of Paper I that the variation in the gas temperature lags the variation in the stellar luminosity by a phase angle equal to $\pi/2 + \tan^{-1}(\omega\tau)$, where $\omega\tau \approx 5.7 \times 10^{-2} r_{15}^{-2}$. Thus the fact that the maser intensity varies in phase with the stellar luminosity is difficult to reconcile with a collisional pump. Furthermore, at $r \geq 10^{16} \text{ cm}$, where both the VLBI measurements and the theoretical calculations suggest that the 1612 MHz OH maser operate, the temperature variations are very small. From equation (26) of Paper I, it follows that at $r = 10^{16} \text{ cm}$ the temperature varies by less than 1 K in response to a 100 percent variation in stellar luminosity. Variations in stellar luminosity might also affect the emission from a collisionally pumped maser if the maser were unsaturated and amplified the stellar radiation. If this were the case, the output intensity of a 1612 MHz OH maser would be expected to vary in direct proportion to the stellar luminosity variations at $\lambda = 18 \text{ cm}$. This hypothesis must be rejected, since it leads to the prediction that only the maser emission from in front of the star should vary whereas observations show proportional variations of both maser emission peaks.

If collisions do not power the maser pump, then radiation must. Two possibilities have to be considered. The maser could be pumped by the absorption of near-infrared (NIR) photons at $\lambda = 2.8 \mu$ which excite the rotational levels of the first excited vibrational state of the OH molecules. The maser could also be pumped by the absorption of far-infrared (FIR) photons which excite the rotational levels of the ground vibrational state of OH. Detailed numerical calculations show that both NIR and FIR pumping can lead to the inversion of the 1612 MHz transition. However, at the OH column densities predicted by the H_2O photodissociation calculations, the rotation-vibrational lines are optically thin, and NIR pumping is not important. Therefore, only the FIR pump cycle is considered here.

b) FIR Pump Cycle

As previously discussed, the maser emission is thought to originate at $r \geq 10^{16} \text{ cm}$ where $n_{\text{H}_2} \lesssim 3 \times 10^5 \text{ cm}^{-3}$ and the dust temperature $T_d \lesssim 300 \text{ K}$. In this environment the collision rate is very low compared with the net derivative decay rates of the excited rotational states.¹ Therefore, most of the OH molecules will be in the ground rotational state. The important pump lines are those which connect the ground rotational state to excited rotational states. These states and the wavelengths of the transitions that connect them to the ground state are (cf. Fig. 1) ${}^2\Pi_{3/2}, J = 5/2 (\lambda = 120 \mu)$; ${}^2\Pi_{1/2}, J = 1/2 (\lambda = 79 \mu)$; ${}^2\Pi_{1/2}, J = 3/2 (\lambda = 53 \mu)$; and ${}^2\Pi_{1/2}, J = 5/2 (\lambda = 35 \mu)$.

The FIR photons which couple the ground rotational state to higher rotational states are emitted by the warm dust grains. With an assumed emissivity $\epsilon_\lambda \propto \lambda^{-1}$ for the dust grains, the radiated spectrum, F_ν , peaks at $\lambda \approx 0.4 T_d^{-1}$, where λ is in centimeters and T is in kelvins. At the temperatures of the dust grains in the region of maser emission ($100 \text{ K} < T_d < 200 \text{ K}$), the photon production rate² in the 35μ line exceeds that in any of the other lines which connect the ground rotational state to excited rotational states.

A simple description of the population flow in the pump cycle can be given by temporarily neglecting the Λ -doubling and hyperfine splitting of the rotational levels. It will be assumed that the lines formed between the rotational states are optically thin with the possible exception of the lines connecting the ground rotational state with excited rotational states. This assumption

¹ For optically thick lines, the net radiative decay rates are smaller than the spontaneous emission rates because of the effects of photon trapping.

² The photon production rate in a line is defined as the rate of photon emission per unit frequency interval multiplied by the line width. Since the line width $\Delta\nu \propto \nu$ for Doppler broadened lines, the photon production rate also peaks at $\lambda \approx 0.4 T_d^{-1}$.

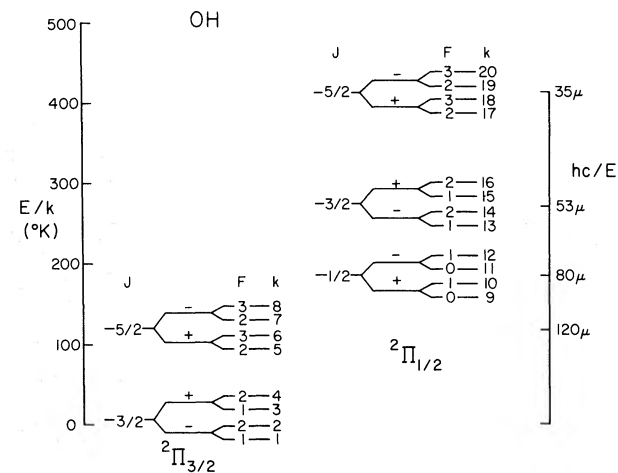


FIG. 1.—The hyperfine-split Λ -doublets in the ground vibrational state are shown above (not to scale). Included are all of the rotational states that are coupled to the ground rotational state by a radiative (dipole) transition.

can be checked against the results of numerical solutions of the equations of statistical equilibrium and radiative transfer in model circumstellar envelopes about OH-IR stars. It is found that the assumption is valid over a significant range of parameters for which strong 1612 MHz inversions are produced. Since the details of the pump cycle are particularly simple when the lines connecting the excited rotational states are optically thin, the discussion below is restricted to this case.

The simplified pump cycle consists of the absorption of a 35μ photon by an OH molecule initially in the ground rotational state which excites the molecule to the $^2\Pi_{1/2}, J = 5/2$ state. The excited molecule returns to the ground rotational state by a series of spontaneous decays. Because the spontaneous decay rates of transitions from the $\Pi_{1/2}$ to the $\Pi_{3/2}$ ladder are much slower (by an order of magnitude or so) than those which proceed directly down the $\Pi_{1/2}$ ladder, the molecule usually follows the route $^2\Pi_{1/2}, J = 5/2 \rightarrow ^2\Pi_{1/2}, J = 3/2 \rightarrow ^2\Pi_{1/2}, J = 1/2$.³ From the $^2\Pi_{1/2}, J = 1/2$ state the only possible decay is to the $^2\Pi_{3/2}, J = 3/2$ state which completes the cycle.

In order to obtain a qualitative understanding of how the $F = 1 \rightarrow F = 2$ transition of the $^2\Pi_{3/2}, J = 3/2$ state is inverted, it is necessary to consider the Λ -doubling and hyperfine splitting of the rotational levels. The symmetry between the upper and lower halves of the Λ -doublets implies that a radiative pump cannot produce a net population transfer across the ground state Λ -doublet.⁴ Only a net transfer of population between the two hyperfine levels of a given half of the Λ -doublet can arise. Thus, in the discussion given below, only one half of each Λ -doublet is considered.

The inversion of the $F = 1 \rightarrow F = 2$ transition can be crudely understood as follows. The absorption of 35μ photons by molecules in the $^2\Pi_{3/2}, J = 3/2$ state selectively depletes the population of the $F = 2$ level relative to that of the $F = 1$ level because the $F = 2$ level couples to both hyperfine levels of $^2\Pi_{1/2}, J = 5/2$ state whereas the $F = 1$ level is only coupled to one of them. The OH molecules return to the ground state mainly from the $^2\Pi_{1/2}, J = 1/2$ state. This final step in the pump cycle selectively overpopulates the $F = 1$ level of the ground rotational state relative to the $F = 2$ level because the $F = 1$ level is connected to both of the hyperfine levels of the $^2\Pi_{1/2}, J = 1/2$ state whereas the $F = 2$ level is only connected to one of them.

³ This statement is only true if, as assumed here, the lines formed in the transitions $^2\Pi_{1/2}, J = 5/2 \rightarrow ^2\Pi_{1/2}, J = 3/2$ and $^2\Pi_{1/2}, J = 3/2 \rightarrow ^2\Pi_{1/2}, J = 1/2$ are optically thin. Otherwise, the net decay rates down the $\Pi_{1/2}$ ladder would be reduced by photon trapping.

⁴ The symmetry is broken by the unequal hyperfine splittings of the upper and lower halves of the Λ -doublets. At sufficiently high temperatures ($T \gtrsim 400$ K) or with sufficiently large velocity gradients, some overlapping of FIR lines between different hyperfine components occurs. In principle, this overlap can give rise to inversion of the main line ($\Delta F = 0$) transitions (Litvak 1969). In the present paper the overlap of the FIR lines is ignored, since it is not an essential feature of the 1612 MHz pump mechanism.

A more detailed look at the pump cycle requires knowledge of the line strengths and optical depths of the pump lines and consideration of the degeneracies of the hyperfine levels. The line strengths and spontaneous emission rates for the rotational transitions are given in Table 1. These line strengths have been used to calculate the population flow in the dominant pump cycle.

Figure 2 illustrates the population flow for the case in which all of the transitions connecting rotational states are optically thin. It is obvious from the figure that in this case the dominant pump cycle does not produce a net transfer of population between the $F = 1$ and $F = 2$ hyperfine levels of the ground rotational state. In fact, each step in the pump cycle transfers population both into and out of the hyperfine levels at rates proportional to their degeneracies. It is easy to show that the same results hold when all of the rotational transitions are included as long as they are all optically thin.

Figure 3 illustrates the population flow for the case in which all of the rotational transitions connecting excited rotational states are optically thin, but those which couple the ground and excited rotational states are optically thick. The excitation temperatures of the transitions which connect levels in the ground and excited rotational states are assumed to be very low ($kT_{ij} \ll h\nu_{ij}$). This is equivalent to the assumption that most of the OH molecules are in the ground rotational state. This assumption implies that the absorption rate is the same in each of the lines which connect the $^2\Pi_{3/2}, J = 3/2$ and $^2\Pi_{1/2}, J = 5/2$ rotational states. It is further assumed that the hyperfine levels of the ground rotational state are populated in proportion to their statistical weights. This assumption implies that the brightness temperatures, and hence the photon emission rates, are the same for both of the lines which connect the $F = 1$ level of the $^2\Pi_{1/2}, J = 1/2$ rotational state to the hyperfine levels of the ground rotational state. The pump cycle illustrated in Figure 3 produces a net transfer of population from the $F = 2$ to the $F = 1$ hyperfine level. The relevant quantity for maser inversion is the population per degenerate sublevel rather than the population per level. The initial step in the pump process, the absorption of 35μ photons by molecules in the $^2\Pi_{3/2}, J = 3/2$ state, removes population at 2 times the rate from the $F = 2$ level as from the $F = 1$ level. Per sublevel, the $F = 2$ level loses population 6/5 times faster than the $F = 1$ level does. In the final step of the pump process, the radiative decay from the $^2\Pi_{1/2}, J = 1/2$ state to the $^2\Pi_{3/2}, J = 3/2$ state, the population of the $F = 1$ level increases at 7/3 times the rate that the population of the $F = 2$ level does. Per sublevel, the population of the $F = 1$ level increases 35/9 times faster than that of the $F = 2$ level. These considerations demonstrate that the most important step in producing the inversion of the $F = 1 \rightarrow F = 2$ transition is the transfer of population from the $^2\Pi_{1/2}, J = 1/2$ state to the $^2\Pi_{3/2}, J = 3/2$ state.

The description of the pump mechanism given in the previous paragraph is strictly valid only if the

TABLE 1A
OH ROTATIONAL TRANSITIONS

$^2\Pi_{\Omega''} \rightarrow ^2\Pi_{\Omega'}$	$J'' \rightarrow J'$	$F'' \rightarrow F'$	$A(s^{-1})$	$\nu(10^{12} \text{ Hz})$	$k'' \rightarrow k'$
$^2\Pi_{3/2} \rightarrow \Pi_{3/2} \dots$	$5/2 \rightarrow 3/2$	$2 \rightarrow 1$	0.1230	2.51	$5 \rightarrow 1, 7 \rightarrow 3$
		$2 \rightarrow 2$	0.0140	2.51	$5 \rightarrow 2, 7 \rightarrow 4$
		$3 \rightarrow 2$	0.1370	2.51	$6 \rightarrow 2, 8 \rightarrow 4$
$^2\Pi_{1/2} \rightarrow ^2\Pi_{3/2} \dots$	$1/2 \rightarrow 3/2$	$0 \rightarrow 1$	0.0351	3.79	$9 \rightarrow 1, 11 \rightarrow 3$
		$1 \rightarrow 1$	0.0059	3.79	$10 \rightarrow 1, 12 \rightarrow 3$
		$1 \rightarrow 2$	0.0292	3.79	$10 \rightarrow 2, 12 \rightarrow 4$
$^2\Pi_{1/2} \rightarrow ^2\Pi_{3/2} \dots$	$3/2 \rightarrow 3/2$	$1 \rightarrow 1$	0.0373	5.63	$15 \rightarrow 1, 13 \rightarrow 3$
		$1 \rightarrow 2$	0.0075	5.63	$15 \rightarrow 2, 13 \rightarrow 4$
		$2 \rightarrow 1$	0.0045	5.63	$16 \rightarrow 1, 14 \rightarrow 3$
		$2 \rightarrow 2$	0.0403	5.63	$16 \rightarrow 2, 14 \rightarrow 4$
$^2\Pi_{1/2} \rightarrow ^2\Pi_{3/2} \dots$	$5/2 \rightarrow 3/2$	$2 \rightarrow 1$	0.0156	8.66	$17 \rightarrow 1, 19 \rightarrow 3$
		$2 \rightarrow 2$	0.0017	8.66	$17 \rightarrow 2, 19 \rightarrow 4$
		$3 \rightarrow 2$	0.0173	8.66	$18 \rightarrow 2, 20 \rightarrow 4$
$^2\Pi_{1/2} \rightarrow ^2\Pi_{3/2} \dots$	$3/2 \rightarrow 5/2$	$1 \rightarrow 2$	0.0090	3.11	$13 \rightarrow 5, 15 \rightarrow 7$
		$2 \rightarrow 2$	0.0006	3.11	$14 \rightarrow 5, 16 \rightarrow 7$
		$2 \rightarrow 3$	0.0084	3.11	$14 \rightarrow 6, 16 \rightarrow 8$
$^2\Pi_{1/2} \rightarrow ^2\Pi_{3/2} \dots$	$5/2 \rightarrow 5/2$	$2 \rightarrow 2$	0.0523	6.16	$19 \rightarrow 5, 17 \rightarrow 7$
		$2 \rightarrow 3$	0.0037	6.16	$19 \rightarrow 6, 17 \rightarrow 8$
		$3 \rightarrow 2$	0.0027	6.16	$20 \rightarrow 5, 18 \rightarrow 7$
		$3 \rightarrow 3$	0.0533	6.16	$20 \rightarrow 6, 18 \rightarrow 8$
$^2\Pi_{1/2} \rightarrow ^2\Pi_{1/2} \dots$	$3/2 \rightarrow 1/2$	$1 \rightarrow 0$	0.0427	1.84	$13 \rightarrow 9, 15 \rightarrow 11$
		$1 \rightarrow 1$	0.0214	1.84	$13 \rightarrow 10, 15 \rightarrow 12$
		$2 \rightarrow 1$	0.0641	1.84	$14 \rightarrow 10, 16 \rightarrow 12$
$^2\Pi_{1/2} \rightarrow ^2\Pi_{1/2} \dots$	$5/2 \rightarrow 3/2$	$2 \rightarrow 1$	0.3150	3.04	$17 \rightarrow 13, 19 \rightarrow 15$
		$2 \rightarrow 2$	0.0350	3.04	$17 \rightarrow 14, 19 \rightarrow 16$
		$3 \rightarrow 2$	0.3500	3.04	$18 \rightarrow 14, 20 \rightarrow 16$

TABLE 1B
OH Λ -DOUBLET TRANSITIONS

$^2\Pi_{\Omega}$	J	$F'' \rightarrow F'$	$A(s^{-1})$	$\nu(10^6 \text{ Hz})$	$k'' \rightarrow k'$
$^2\Pi_{3/2} \dots$	$3/2$	$1 \rightarrow 2$	1.289(-11)	1612.231	$3 \rightarrow 2$
		$1 \rightarrow 1$	7.103(-11)	1665.401	$3 \rightarrow 1$
		$2 \rightarrow 2$	7.698(-11)	1667.358	$4 \rightarrow 2$
		$2 \rightarrow 1$	0.940(-11)	1720.533	$4 \rightarrow 1$
$^2\Pi_{3/2} \dots$	$5/2$	$2 \rightarrow 3$	1.087(-10)	6016.746	$7 \rightarrow 6$
		$2 \rightarrow 2$	1.532(-09)	6030.739	$7 \rightarrow 5$
		$3 \rightarrow 3$	1.567(-09)	6035.085	$8 \rightarrow 6$
		$3 \rightarrow 2$	7.887(-11)	6049.084	$6 \rightarrow 5$
$^2\Pi_{1/2} \dots$	$1/2$	$0 \rightarrow 1$	1.081(-09)	4660.242	$11 \rightarrow 10$
		$1 \rightarrow 1$	7.633(-10)	4750.656	$12 \rightarrow 10$
		$1 \rightarrow 0$	3.852(-10)	4765.562	$12 \rightarrow 9$
$^2\Pi_{1/2} \dots$	$3/2$	$1 \rightarrow 2$	1.863(-10)	7749.168	$15 \rightarrow 14$
		$1 \rightarrow 1$	9.358(-10)	7761.329	$15 \rightarrow 13$
		$2 \rightarrow 2$	1.034(-09)	7819.821	$16 \rightarrow 14$
		$2 \rightarrow 1$	1.154(-10)	7831.830	$16 \rightarrow 13$
$^2\Pi_{1/2} \dots$	$5/2$	$2 \rightarrow 3$	4.298(-11)	8118.052	$19 \rightarrow 18$
		$2 \rightarrow 2$	5.986(-10)	8135.868	$19 \rightarrow 17$
		$3 \rightarrow 3$	6.230(-10)	8189.586	$20 \rightarrow 18$
		$3 \rightarrow 2$	3.136(-11)	8207.401	$20 \rightarrow 17$

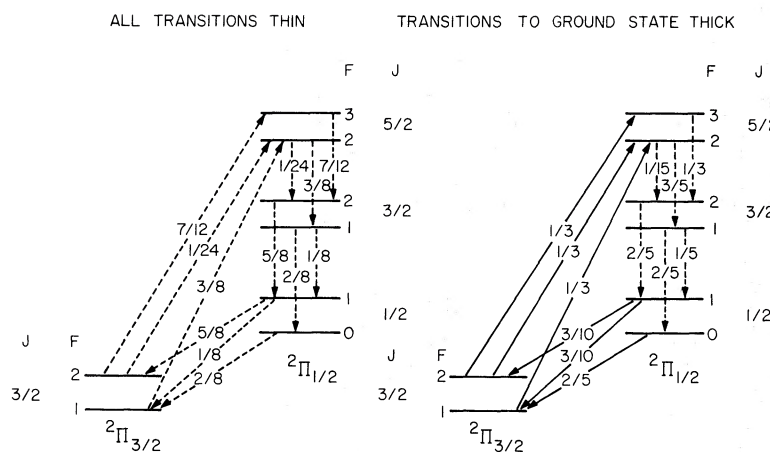


FIG. 2

FIG. 3

FIG. 2.—The population flow is shown following the absorption of 35μ photons by OH molecules in the ${}^2\Pi_{3/2}$, $J = 3/2$ rotational state. The relative transition rates are calculated for the case in which all of the rotational transitions are optically thin (*dashed arrows*). *No net transfer of population between the hyperfine levels in the ground rotational state occurs.* Because of the symmetry between the upper and lower halves of the Λ -doublets, only one-half of each doublet is shown. The total absorption rate out of each half of the ${}^2\Pi_{3/2}$, $J = 3/2$ Λ -doublet is normalized to unity.

FIG. 3.—The population flow is shown following the absorption of 35μ photons by OH molecules in the $^2\Pi_{3/2}, J = 3/2$ rotational state. The relative transition rates are calculated assuming that the transitions between excited rotational states are optically thin (dashed arrows) and the transitions between the excited rotational states and the ground rotational state are optically thick (solid arrows). There is a net transfer of population from the $F = 2$ to the $F = 1$ hyperfine level of the ground rotational state. Because of the symmetry between the upper and lower halves of the Λ -doublets, only one-half of each doublet is shown. The total absorption rate out of each half of the $^2\Pi_{3/2}, J = 3/2$ Λ -doublet is normalized to unity.

hyperfine levels of the ground rotational state are populated according to their statistical weights. Of course, by transferring population from the $F = 2$ to the $F = 1$ hyperfine level, the pump process tends to create unequal sublevel populations in the $F = 1$ and $F = 2$ hyperfine levels. Furthermore, if the maser radiation saturates the 1612 MHz transition, it produces a net transfer of population from the upper to the lower half of the ground state Λ -doublet. Numerical calculations are required to follow the population flow when the hyperfine levels of the ground rotational state are not populated according to their statistical weights. These calculations, which will be described shortly, show that when the maser is saturated there is a net transfer of population from the lower to the upper halves of the Λ -doublets by means of $\Delta J = 0$ transitions. The most important transitions are those between the $^2\Pi_{3/2}$, $J = 3/2$ and $^2\Pi_{1/2}$, $J = 3/2$ rotational states. These radiative rotational transitions almost exactly balance the downward transitions across the ground state Λ -doublet which are induced by the maser photons. A small additional transfer of population from the lower to the upper half of the ground state Λ -doublet is produced by collisions.

Up to now the discussion of the pump mechanism has ignored nonlocal effects. However, there is one such effect which is of possible importance to the inversion of the 1612 MHz transition. It arises as follows. Due to the combined effects of the spherical divergence of the gas as it streams away from the central star and to its radial acceleration, the gas is in

a state of expansion about every point. Thus, as seen by the local gas, the frequency of a photon traversing the circumstellar envelope suffers a redshift which increases with time. Since several closely spaced FIR transitions may connect a pair of rotational states, it is possible for a photon which interacts in one of these transitions at some point to subsequently interact in a slightly lower frequency transition at another point in the circumstellar envelope. Clearly, these nonlocal interactions are only significant for lines which have appreciable optical depths such as those which link the ground rotational state to excited rotational states. The most important example of this type involves the decays from the levels of the ${}^2\Pi_{1/2}, J = 1/2$ state to the levels of the ${}^2\Pi_{3/2}, J = 3/2$ state. Because of the very unequal hyperfine splittings of the upper and lower halves of the ${}^2\Pi_{1/2}, J = 1/2$ Λ -doublet, the nonlocal interactions do not affect the population transfer among the hyperfine levels of the upper and lower halves of the Λ -doublets symmetrically.

Consider first the case of transitions between the upper halves of the Λ -doublets. In order of decreasing frequency, these transitions are $F' = 1 \rightarrow F = 1$, $F' = 1 \rightarrow F = 2$, and $F' = 0 \rightarrow F = 1$ where the primes denote levels in the ${}^2\Pi_{1/2}, J = 1/2$ state. The redshifts required to take a photon from the $F' = 1 \rightarrow F = 1$ transition to the $F' = 1 \rightarrow F = 2$ transition and from the $F' = 1 \rightarrow F = 2$ transition to the $F' = 0 \rightarrow F = 1$ transition are 4.4 km s^{-1} and 2.8 km s^{-1} , respectively. The principal effect on the population flow arises because photons which are

emitted at one point in a $F' = 1 \rightarrow F = 1$ transition may subsequently be absorbed at another point and produce a $F = 2 \rightarrow F' = 1$ transition. This process reduces the net rate at which population enters the $F = 2$ level with respect to that at which it enters the $F = 1$ level.

Next, consider the case of transitions between the lower halves of the Λ -doublets. In order of decreasing frequency, the transitions are $F' = 1 \rightarrow F = 1$, $F' = 0 \rightarrow F = 1$, and $F' = 1 \rightarrow F = 2$. The redshifts required to take a photon from the $F' = 1 \rightarrow F = 1$ transition to the $F' = 0 \rightarrow F = 1$ transition and from the $F' = 0 \rightarrow F = 1$ transition to the $F' = 1 \rightarrow F = 2$ transition are 1.2 km s^{-1} and 3.0 km s^{-1} , respectively. The principal effect of the nonlocal interactions is that photons emitted in the $F' = 0 \rightarrow F = 1$ transition at one point may subsequently be absorbed and produce a $F = 2 \rightarrow F' = 1$ transition at another point. This reduces the relative rate of the net population flow into the $F = 2$ level with respect to that into the $F = 1$ level.

The upshot of these nonlocal interactions is to enhance the efficiency of the 1612 MHz pump. Similar nonlocal effects may be worked out for other rotational transitions, but they are less important than those just described. Although the nonlocal interactions may produce significant effects, they are difficult to account for quantitatively, and therefore they are neglected in the detailed calculations of the pump cycle which are outlined in §§ IVc and IVd.

c) Equations of Radiative Transfer and Statistical Equilibrium

It would be extremely difficult to obtain a general solution of the equations of radiative transfer and statistical equilibrium in an expanding circumstellar envelope. Fortunately, in the limit that the thermal velocity of the molecules is much smaller than the expansion velocity, a simple approximate method of solving the equations of radiative transfer has been developed by Sobolev (1960) and extended by Castor (1970) and Lucy (1971). These authors prove that in this limit the value of the mean intensity at any point, when integrated over the line profile, depends only upon the local value of the source function, the external continuum radiation field, and the probability that a photon emitted at that point will escape without further interaction. Thus the rates of absorption and stimulated emission are determined by two local quantities, the source function and the escape probability, and local expressions for the radiative transition rates may be used in place of the solutions of the complicated nonlocal equations of radiative transfer. This paper follows the treatment by Castor (1970), and his results are used in the equations of statistical equilibrium.

The probability that a photon emitted in a transition between levels i and j will escape without further interaction is given by

$$\beta_{ij}(r) = \int \frac{d\Omega}{4\pi} \beta_{ij}(r, \mu) = \int \frac{d\Omega}{4\pi} \left\{ \frac{1 - \exp[-\tau_{ij}(r, \mu)]}{\tau_{ij}(r, \mu)} \right\}, \quad (7)$$

where

$$\tau_{ij}(r, \mu) = \frac{\hat{\tau}_{ij}}{1 + \mu^2(d \ln v / d \ln r - 1)} \quad (8)$$

is the optical depth in the direction which makes an angle $\theta = \cos^{-1} \mu$ with the radius vector. The optical depth parameter

$$\hat{\tau}_{ij} = \frac{hcr}{4\pi v} B_{ij} g_i (n_j - n_i), \quad (9)$$

where n_k is the number density per sublevel of OH molecules in level k , g_k is the level degeneracy, and B_{ij} is the Einstein coefficient.⁵

From the local expressions for the net radiative transition rates, the equations of statistical equilibrium may be shown to take the form (note that $E_i > E_j$ for $i > j$)

$$\begin{aligned} \frac{dn_k}{dt} = & \sum_{j > k} \frac{g_j}{g_k} A_{jk} \left\{ \beta_{jk} \left[n_j - \frac{(n_k - n_j)}{\exp(h\nu_{jk}/kT_{\text{BB}}) - 1} \right] \right. \\ & \left. - D_{jk}(n_k - n_j) \right\} \\ & + Cg_j \left[n_j - n_k \exp\left(-\frac{h\nu}{kT} jk\right) \right] \\ & - \sum_{j < k} A_{kj} \left\{ \beta_{kj} \left[n_k - \frac{(n_j - n_k)}{\exp(h\nu_{kj}/kT_{\text{BB}}) - 1} \right] \right. \\ & \left. - D_{kj}(n_j - n_k) \right\} \\ & - Cg_j \left[n_k - n_j \exp\left(-\frac{h\nu}{kT} kj\right) \right], \end{aligned} \quad (10)$$

where $g_i A_{ij} D_{ij}(n_j - n_i)$, with

$$D_{ij}(r) = \frac{1}{2} \int_{-1}^1 d\mu \left[\beta_{ij}(r, \mu) \int_{-\mu r}^{\infty} D(r', \nu_{ij}) dz' \right], \quad (11)$$

is the contribution to the radiative transition rate between levels i and j due to photons emitted by the warm dust grains and T_{BB} is the temperature of the cosmic background radiation.

The coefficient $\beta_{ij} A_{ij}$ which appears in equation (10) is the net radiative decay rate from level i to level j . The β_{ij} factor is present because only those spontaneous emissions that give rise to a photon which escapes contribute to the net transfer of population from level i to level j .

The quantity D_{ij} is equal to the photon occupation number in the ij line averaged over both direction and the line profile (i.e., D_{ij} is the product of $c^2/2h^3$ and the mean intensity in the ij line averaged over the line profile). With this definition, the integral expression for D_{ij} given by equation (11) is easy to decipher. The

⁵ From eqs. (7)–(9) it follows directly that $\beta_{ij} A_{ij} g_i n_i$ is independent of A_{ij} for an optically thick transition. This confirms the assertion in § IVb to the effect that the photon emission rate in an optically thick transition is independent of the line strength.

factor $D(r, \nu)$ is the rate at which energy is emitted by the dust grains per unit volume, per unit frequency interval, per unit solid angle, divided by $2h\nu^3/c^2$. It may be written as

$$D(r, \nu) = \frac{\epsilon_d(\nu)\sigma_d n_d(r)}{\{\exp[h\nu/kT_d(r)] - 1\}}, \quad (12)$$

where $\epsilon_d(\nu)$ is the dust emissivity. In all applications

$$\epsilon_d(\nu) = \frac{2\pi a\nu}{c} \quad (13)$$

with $a = 10^{-5}$ cm will be used. The first integration in the expression for $D_{ij}(r)$ is along a ray which intersects the radius vector at an angle θ at radial distance r (note that $z = \mu r$). The product of this integral and the factor $\beta_{ij}(r, \mu)$ (which is the photon escape probability along the ray) gives the profile averaged photon occupation number due to dust grain emission along the ray. The second integration just averages the photon occupation number over all directions. The derivation of the expression for $D_{ij}(r)$ given by equation (11) follows directly from the equations in Castor (1970).

The temperature of the dust grains is given by

$$T_d = \left(\frac{LT_e}{16\pi\sigma r^2} \right)^{1/5}. \quad (14)$$

For OH-IR Mira variables, $L \approx 10^4 L_\odot$ and $T_e \approx 2 \times 10^3$ K. Thus $T_d \approx 195 r_{16}^{-2/5}$ K.

It is easy to show from equations (11), (12), and (14) that the principal contributions to $D_{ij}(r)$ come from $r/3 < r' < 3r$. Contributions from $r' \gg r$ are negligible because $n_d(r') \propto r'^{-2}$, and contributions from $r' \ll r$ are unimportant because these inner regions subtend such a small solid angle at r ($\Delta\Omega \approx 4\pi r'^2/r^2$). Since the dust temperature varies slowly with r , $T_d \propto r^{-2/5}$, it is a reasonable approximation to set $T_d(r') = T_d(r)$ in the expression for $D(r', \nu)$ when evaluating $D_{ij}(r)$ from equation (11). This is the procedure that is followed in the paper. It is then possible to evaluate D_{ij} analytically when $\tau_{ij}(r, \mu)$ is either $\ll 1$ or $\gg 1$ for $-1 \leq \mu \leq 1$. For intermediate cases in which $\tau_{ij}(r, \mu) = 1$ at some value of μ , $D_{ij}(r)$ must be calculated numerically. Fortunately, simple analytic fits to the numerical values of $D_{ij}(r)$ are easily devised.

The form of the collision terms in equation (10) is essentially a guess. It is assumed that the collisional cross sections for all rotational transitions are equal to 10^{-15} cm $^{-2}$. The probability of reaching any particular hyperfine level within a given rotational state is taken to be proportional to the statistical weight of the hyperfine level.

d) Numerical Calculations

The equations of statistical equilibrium (eqs. [10]) are solved numerically using Newton's method. The convergence criterion is that $\Delta n_i/n_i < 10^{-4}$ on successive iterations. The OH energy levels included in the calculations are all those which directly couple by FIR transitions to levels in the ground rotational state.

These are the hyperfine levels of the $J = 3/2$ and $J = 5/2$ rotational states on the ${}^2\Pi_{3/2}$ ladder and those of the $J = 1/2$, $J = 3/2$, and $J = 5/2$ rotational states on the ${}^2\Pi_{1/2}$ ladder (cf. Fig. 1).

The effects of saturation in any maser transition are automatically accounted for because the escape probability formalism works just as well for inverted as for anti-inverted transitions. In either case, the specific intensity averaged over the line profile is given by (neglecting dust grain emission and the cosmic background radiation)

$$I_{ij}(r, \mu) = \frac{2h\nu_{ij}^3}{c^2} \frac{n_i}{(n_j - n_i)} [1 - \beta_{ij}(r, \mu)]. \quad (15)$$

An expression for the mean intensity can be obtained from equation (15) by replacing $\beta_{ij}(r, \mu)$ with $\beta_{ij}(r)$. For inverted transitions, $n_i > n_j$ and $\tau_{ij} < 0$. If the gain is large, $\beta_{ij} \gg 1$.

The parameter values used in the numerical calculations are taken from Paper I. They are the following: $M = M_\odot = 2 \times 10^{33}$ gm, $L = 10^4 L_\odot = 4 \times 10^{37}$ ergs s $^{-1}$, $R = 6 \times 10^{13}$ cm, $T_e = 2 \times 10^3$ K, $Q = 1/2$. The optical depth due to dust grains from $r = 10^{16}$ cm to $r = \infty$, $\tau_{16} = (Qn_d\sigma r)_{r=10^{16}\text{ cm}} = 0.07$. Although calculations were run for several values of the radial distance r , only the results for $r = 3 \times 10^{16}$ cm are given in detail. At $r = 3 \times 10^{16}$ cm, the standard model has $n_H = n_{H_2} = 2 \times 10^4$ cm $^{-3}$, $T = 50$ K, $T_d = 125$ K, and $v = 20$ km s $^{-1}$. From equation (6), $d \ln v/d \ln r = 8 \times 10^{-3}$. Computations were performed with these standard parameters for values of n_{OH} in the range 10^{-2} cm $^{-3} < n_{OH} < 10$ cm $^{-3}$. The results are presented in Table 2 and Figure 4.

TABLE 2
SUBLEVEL POPULATIONS FOR $n_{OH} = 4$ cm $^{-3}$
AT $r = 3 \times 10^{16}$ cm

${}^2\Pi_\alpha$	J	F	k	n_k (cm $^{-3}$)
${}^2\Pi_{3/2} \dots \dots$	3/2	1 ⁻	1	0.2698
		2 ⁻	2	0.2500
		1 ⁺	3	0.2514
		2 ⁺	4	0.2364
${}^2\Pi_{3/2} \dots \dots$	5/2	2 ⁺	5	1.015(-4)
		3 ⁺	6	1.804(-4)
		2 ⁻	7	9.544(-5)
		3 ⁻	8	1.704(-4)
${}^2\Pi_{1/2} \dots \dots$	1/2	0 ⁺	9	9.783(-5)
		1 ⁺	10	1.107(-4)
		0 ⁻	11	9.171(-5)
		1 ⁻	12	1.042(-4)
${}^2\Pi_{1/2} \dots \dots$	3/2	1 ⁻	13	4.500(-6)
		2 ⁻	14	3.384(-6)
		1 ⁺	15	4.523(-6)
		2 ⁺	16	3.366(-6)
${}^2\Pi_{1/2} \dots \dots$	5/2	2 ⁺	17	2.356(-7)
		3 ⁺	18	1.804(-7)
		2 ⁻	19	2.268(-7)
		3 ⁻	20	1.739(-7)

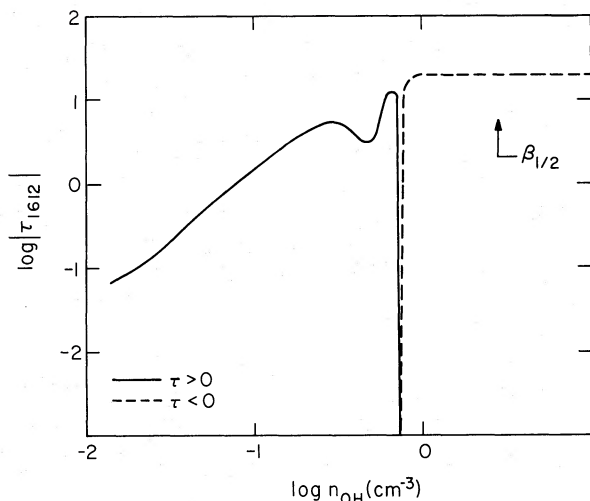


FIG. 4.—The radial optical depth in the 1612 MHz transition is plotted as a function of the OH abundance. The optical thickness of the circumstellar dust is denoted by τ_{16} . The 1612 MHz transition is inverted and saturated for $n_{\text{OH}} \gtrsim 1 \text{ cm}^{-3}$. The escape probability in the weakest transition between the $^2\Pi_{1/2}, J = 1/2$ and $^2\Pi_{3/2}, J = 3/2$ rotational states is equal to 0.5 (indicated by $\beta_{1/2}$ on the figure) at $n_{\text{OH}} \approx 3 \text{ cm}^{-3}$.

Table 2 contains the fractional populations per degenerate sublevel for one solution which is typical of those for which the 1612 MHz maser is saturated. The computed populations confirm the assumption made previously that most of the population is in the ground rotational state. It is evident that some of the transitions across the Λ -doublets of excited rotational states are inverted. In particular, the 6049 MHz, $F = 3^- \rightarrow F = 2^+$ transition in the $^2\Pi_{3/2}, J = 5/2$ rotational state is strongly inverted. However, the gain in this transition is not large enough for it to produce observable maser emission. In general, it seems unlikely that observable excited state OH masers operate in the outer regions of circumstellar envelopes about Mira variables unless the OH densities there are much higher than those estimated in Paper I.

Figure 4 shows that the 1612 MHz transition is inverted and saturated for $n_{\text{OH}} \gtrsim 1 \text{ cm}^{-3}$. The value of the escape probability for the transition between the $F = 1$ level of the $^2\Pi_{1/2}, J = 1/2$ state and the $F = 1$ level of the $^2\Pi_{3/2}, J = 3/2$ state is equal to 0.5 at $n_{\text{OH}} \approx 3 \text{ cm}^{-3}$. This is the weakest line linking these rotational states. From the arguments in § IVb and the diagrams in Figures 4 and 5, it is clear that this is the crucial line that must be optically thick for the 1612 MHz transition to be strongly inverted. The fact that the numerical calculations show that this line becomes optically thick at the lowest OH density for which the 1612 MHz transition is strongly inverted confirms the qualitative description of the pump cycle presented in § IVb.

There is one aspect of the qualitative description of the maser pump cycle described in § IVb which is not faithfully reproduced in the numerical calculations. That is, the transition between the $F = 2$ level of the $^2\Pi_{3/2}, J = 3/2$ rotational state and the $F = 2$ level of the $^2\Pi_{1/2}, J = 5/2$ state is optically thin for $n_{\text{OH}} <$

20 cm^{-3} . Consequently, the absorption of 35μ photons by molecules in the $^2\Pi_{3/2}, J = 3/2$ state tends to weakly anti-invert the 1612 MHz transition. However, the transitions from the $^2\Pi_{1/2}, J = 1/2$ state to the $^2\Pi_{3/2}, J = 3/2$ state dominate when they are optically thick and the 1612 MHz transition is inverted in the manner described in § IVb.

Although detailed results are only presented for one set of parameter values, several additional calculations using different parameter values were performed in the course of this investigation. A few of the interesting results from these other calculations are summarized here.

Perhaps the most significant results concern the importance of collisions in the pump cycle. In the standard calculation, it was found that collisions did not play an important role in the population transfer. To test for the effects of collisions on the pump mechanism, a series of calculations was carried out in which all the parameters were kept at their standard values except for the hydrogen density which was increased above the standard value of $n_{\text{H}} = n_{\text{H}_2} = 2 \times 10^4 \text{ cm}^{-3}$. These calculations show that for $n_{\text{H}} = n_{\text{H}_2} \gtrsim 4 \times 10^5 \text{ cm}^{-3}$, the 1612 MHz inversion is quenched by collisions. The principal effect of the collisions is to excite OH molecules from the $^2\Pi_{3/2}, J = 3/2$ state to the $^2\Pi_{3/2}, J = 5/2$ state. The radiative decays from the $^2\Pi_{3/2}, J = 5/2$ state to the $^2\Pi_{3/2}, J = 3/2$ state tend to invert the 1720 MHz transition and thus quench the 1612 MHz inversion. In fact, in some cases the collisions produced strong 1720 MHz inversions. However, as the 1720 MHz inversion depends upon the highly uncertain form chosen for the collisional cross sections, it is not clear that it can arise in nature.

Another calculation was carried out with parameter values appropriate to $r = 10^{16} \text{ cm}$ as determined by the results in Paper I. These parameter values are $n_{\text{H}} = n_{\text{H}_2} = 2 \times 10^5 \text{ cm}^{-3}$, $T = 125 \text{ K}$, $T_d = 200 \text{ K}$, and $d \ln v/d \ln r = 2 \times 10^{-2}$. It was found that the 1612 MHz transition is inverted for $n_{\text{OH}} \gtrsim 7 \text{ cm}^{-3}$.

Finally, a calculation was performed using all of the standard parameter values except for $d \ln v/d \ln r$ which was increased from 8×10^{-3} to 3×10^{-2} . The results in this case are very similar to those of the standard case. A 1612 MHz inversion occurs for $n_{\text{OH}} \gtrsim 1 \text{ cm}^{-3}$. However, saturation only occurs for $n_{\text{OH}} \gtrsim 3 \text{ cm}^{-3}$ unlike the standard case in which it occurs for $n_{\text{OH}} > 1 \text{ cm}^{-3}$.

V. DISCUSSION

a) Apparent Source Size

The specific intensity of the emergent maser radiation is

$$I_{ij}(r, \mu) = \frac{2h\nu_{ij}^3}{c^2} \left[\left\{ 1 - \exp[-\tau_{ij}(r, \mu)] \right\} \left(\frac{n_i}{n_j - n_i} \right) + \exp[-\tau_{ij}(r, \mu)] \left[\frac{1}{\exp(h\nu_{ij}/kT_{\text{BB}}) - 1} \right] \right]. \quad (16)$$

Note that the above expression gives $I_{ij}(r, \mu)$ at a frequency which is a few thermal Doppler widths below (if $\mu > 0$) or above (if $\mu < 0$) the resonant frequency at r . As such, it differs from the expression for the specific intensity averaged over the line profile which is given by equation (15). Equation (16) may be written in a simpler form in terms of the brightness temperature $T_b(r, \mu)$ and the excitation temperature T_{ex} as

$$T_b(r, \mu) = (|T_{\text{ex}}| + T_{\text{BB}}) \exp |\tau_{ij}(r, \mu)| . \quad (17)$$

In deriving equation (17), the relations

$$\exp [-\tau_{ij}(r, \mu)] \gg 1, \quad kT_{\text{BB}}/\hbar\nu_{ij} \gg 1$$

and $k|T_{\text{ex}}|/\hbar\nu_{ij} \gg 1$ are used (note that $\hbar\nu_{ij}/k \approx 0.08$ K for $\nu_{ij} = 1612$ MHz).

The maser gain is largest in the radial direction ($\mu^2 = 1$), since that is the direction along which the line of sight velocity changes most slowly (if $|d \ln v/d \ln r| < 1$). From equations (7), (8), and (15), it follows that the specific intensity falls below its peak value by a factor of e^{-1} at

$$\theta = \left(\frac{1}{|\tau_{ij}(r, \pm 1)|} \frac{d \ln v}{d \ln r} \right)^{1/2} . \quad (18)$$

For the best estimate parameters appropriate to the 1612 MHz maser emission from OH-IR stars, $\theta = 2 \times 10^{-2}$. The apparent diameters of the maser spots are then $2\theta r \approx 1.2 \times 10^{15}$ cm.

The derivation of the apparent source size is based on the assumption that spontaneous emission and the cosmic background are the only sources of input radiation to the maser. This assumption is not entirely correct. The central star may also be an important source of input radiation. As a result, the lower velocity emission feature should contain a component whose angular diameter is equal to the angular diameter of the stellar photosphere. The fraction of the total flux in the low-velocity emission peak that is contained in this component of small angular diameter is given by the relation

$$f = \frac{T^* \phi^2}{(|T_{\text{ex}}| + T_{\text{BB}})\theta^2 + T^* \phi^2} , \quad (19)$$

where $\phi = R/r$ is the angle subtended by the stellar radius R at the region of maser emission r and T^* is the brightness temperature of the stellar photosphere at $\lambda = 18$ cm. As a first guess, T^* might be set equal to $T_e \approx 2000$ K, since the electron density in the photosphere of a giant or a supergiant star is high enough to produce a large free-free opacity at centimeter wavelengths. With a stellar radius $R \approx 6 \times 10^{13}$ cm and $r \approx 3 \times 10^{16}$ cm, $\phi \sim 2 \times 10^{-3}$ as compared with the previously calculated value of $\theta \approx 2 \times 10^{-2}$. Finally, with the best estimate parameters for OH-IR stars, $|T_{\text{ex}}| \approx 14$ K (cf. Table 2). These numerical parameters combine to yield $f \approx 0.5$.

The predicted value of f is in conflict with the finding

by Reid and Muhleman (1975) that no more than 10 percent of the flux from either emission peak in IRC +10011 is contained in a component smaller than $0''1$. The reason for the discrepancy between theory and observation is not understood. It may merely reflect a minor error in the maser model, or it may indicate a deeper lack of understanding of maser amplification. One possibility of the former type is that the assumption of a smooth radial outflow from the central star is not quite correct and that sizable nonradial components of velocity are present. If these velocity components are as large as θv_∞ , then the direction of maximum gain might not pass through the central star. Hence, the amplification of the stellar radiation would be smaller than assumed in equation (19). The existence of sizable nonradial velocities and other inhomogeneities in the circumstellar envelopes surrounding OH-IR supergiant stars is suggested by maps of the positions of the masers in NML Cyg, VY CMa, and VX Sgr (Masheder, Booth, and Davies, 1974). These maps show that the individual masers are grouped in clusters with angular diameters of a few arcseconds.

b) Line Shape and Emitted Power

The maser line shape is determined by the radial velocity gradient in the circumstellar envelope and to a lesser extent by the thermal velocity of the OH molecules. The angular spread of the maser radiation emitted at r results in a contribution of order $\delta v = \theta^2 v_\infty/2$ to the velocity width. Since δv is generally much smaller than the thermal velocity of the OH molecules, it may be neglected.

An analytic derivation of the line shape is possible if a few idealizations and approximations are adopted. Foremost among them is the assumption of a smooth radial flow of gas which is accelerated by radiation pressure acting on dust grains. It is also assumed that the maser is saturated. This assumption is consistent with observations which show that the fractional intensity variation of a 1612 MHz maser never exceeds the fractional intensity variation of the infrared emission from the central star or its surrounding dust shell (Harvey *et al.* 1974). The final assumption is that, at any point, the rate of emission of 1612 MHz maser photons per unit volume is directly proportional to the local rate of emission of 35μ photons per unit volume. Since the pump lines are optically thick, the absorption rate of pump photons is directly proportional to their emission rate. The numerical calculations show that when the pump lines are optically thick and the maser is saturated, about four 35μ photons are absorbed in each of the pump lines for every 1612 MHz photon that is emitted. If the aforementioned assumptions are correct, the emission rate of maser photons per unit volume where the maser is saturated is proportional to $n_d(r)$. The flux density of maser photons emitted from gas moving with radial velocity $v(r)$ is then proportional to $n_d(r)r^2 dr/dv$. Since $r^2 n_d(r)$ is independent of r , the line profile is pro-

portional to dr/dv . From equation (6), it then follows that the observed line profiles should have the form

$$S_v(v) = \frac{A}{(v_\infty - v)^2}, \quad (20)$$

up to some v_{\max} which is very close to v_∞ . For $v > v_{\max}$, the line intensity should decrease abruptly. The difference between v_{\max} and v_∞ is probably determined by either the thermal velocity of the OH molecules or by the local turbulent velocities. The existence of a maximum $v(r)$, which is asymptotically approached at large r , provides a natural explanation for the abrupt outer edges and more gradually tapering inner edges of the maser line profiles.⁶

c) Maser Luminosity

The numerical calculations show that when the 1612 MHz maser is saturated, several 35μ photons are absorbed in each pump line for every maser photon that is emitted. This result can be compared with observations of FIR and maser radiation from OH-IR stars, although several complicating factors hinder the comparison. The first is that, as yet, there are no observations of OH-IR stars at 35μ so that 35μ flux densities must be estimated by extrapolation from the flux densities at 10μ and 20μ . Even if the 35μ flux densities were known, it would still be necessary to estimate the bandwidth over which the OH molecules absorb the 35μ photons. Clearly, the line of sight velocity varies by a value of order v_∞ along a chord which passes through the outer part of the circumstellar envelope where the 1612 MHz maser operates. Thus photons emitted by dust grains in this region can be absorbed over a bandwidth of order vv_∞/c . However, within the maser region, the line of sight velocity along a radial path only changes by the velocity width of the maser lines. For IRC +10011, the velocity widths of the maser lines are about 1 km s^{-1} compared with 20 km s^{-1} for v_∞ . Thus the absorption bandwidth for pump photons emitted close to the star is much smaller than that for photons emitted in the region where the maser operates. The rate of emission of pump photons per unit frequency per unit volume in a spherical shell of thickness Δr about r is proportional to $n_d(r)r^2B_v(T_d)\Delta r$ and therefore to $B_v(T_d)\Delta r$, since $n_d(r)r^2$ is constant. The value of $B_v(T_d)$ evaluated at $v = 8.6 \times 10^{12} \text{ Hz}$, the pump frequency, decreases by a factor of 30 between $T_d = 650 \text{ K}$ and $T_d = 125 \text{ K}$. These values of T_d are estimates for the inner part of the dust shell, at $r = 5 \times 10^{14} \text{ cm}$, and for the maser region, at $r = 3 \times 10^{16} \text{ cm}$. Since most of the 35μ photons are emitted from well inside the maser region, an accurate deduction of the effective bandwidth for

⁶ Kwok, Gilman, and Woolf (1974) have reached a similar conclusion concerning the OH emission profiles. However, they assume that the emission rate per unit volume of maser photons is proportional to n_{OH} . This assumption is incorrect for saturated masers which have photon emission rates per unit volume proportional to n_d . Nevertheless, the line profiles calculated by Kwok, Gilman, and Woolf (1974) are correct because they assume $n_{\text{OH}} \propto n_d$ in the region of maser emission.

absorption of 35μ pump photons can only be obtained by model calculations.

In spite of all the difficulties involved in relating the infrared and maser fluxes from OH-IR stars, the observational results are very encouraging. In general, the estimated 35μ fluxes appear to be adequate to power the maser pumps (Hyland *et al.* 1972).⁷

d) Comparison with Litvak's Calculations: Is the 1612 MHz Maser Pumped by NIR or by FIR Photons?

Litvak (1969) and Litvak and Dickenson (1972) have made calculations of both NIR and FIR pumping of OH masers. Litvak (1969) pointed out that only satellite line ($|\Delta F| = 1$) transitions could be inverted by infrared pumping if the FIR lines between different hyperfine levels did not overlap. He also clearly recognized the importance of photon trapping in determining the population flow among the OH energy levels. However, the conclusions reached by Litvak (1969) and Litvak and Dickenson (1972) concerning the pump mechanism differ from those presented in this paper. Both Litvak (1969) and Litvak and Dickenson (1972) conclude that the 1612 MHz masers are pumped by NIR photons $\lambda = 2.8 \mu$. In fact, Litvak (1969) suggests that pumping by an external FIR source will invert the 1720 MHz transition. Because the physical model for the OH maser clouds assumed by Litvak (1969) is so different from the one adopted in this paper, it is difficult to make meaningful comparisons between his work and the results presented here. In particular, Litvak (1969) neglects velocity gradients in the cloud and solves the one dimensional equation of radiative transfer for the infrared line intensities. In some cases, he finds that the 1612 MHz and 1720 MHz transitions are inverted on opposite sides of a cloud. The local treatment of radiative transfer applied in this paper is incapable of treating such cases which arise because of the differential absorption of the incident radiation in the pump lines as a function of depth in the cloud.

Litvak and Dickenson (1972) find that the 1612 MHz transition is strongly inverted by NIR pumping for OH column densities of order 10^{18} cm^{-2} or greater. They point out that this result only applies if the correct value for the vibration-rotational transition moment is somewhat larger than recent investigations indicate. Otherwise OH column densities greater than 10^{18} cm^{-2} are required to achieve strong 1612 MHz inversions, and collisional quenching of the inversion is hard to avoid. Investigations of NIR pumping carried out as part of this study support the conclusions reached by Litvak and Dickenson (1972). However, the OH column densities required to invert the 1612 MHz transition (10^{18} cm^{-2}) are greater than those which can arise from the photodissociation or collisional dissociation of H₂O in the circumstellar envelopes about stars whose mass loss rates $\dot{M} \approx 3 \times 10^{-5} M_\odot \text{ yr}^{-1}$. The large OH column densities are necessary

⁷ Note that Hyland *et al.* (1972) underestimate the emission rate of 35μ pump photons because they assume equal fractional line widths ($\Delta\nu/\nu$) for the maser and the pump lines.

because the line strengths of the vibration-rotational transitions are so small. The NIR pump inverts the 1612 MHz transition in essentially the same manner that the FIR pump does. In both cases, the crucial transitions are those from the $^2\Pi_{1/2}, J = 1/2$ state to the $^2\Pi_{3/2}, J = 3/2$ state. These transitions tend to invert the 1612 MHz transition when they are optically thick. However, when transitions between the $^2\Pi_{3/2}, J = 3/2$ rotational state of the ground vibrational state and the rotational states in the first excited vibrational state are optically thin, the absorption of 2.8μ photons preferentially excites the $^2\Pi_{3/2}$ rotational states of the first excited vibrational state. This occurs because the line strengths of transitions between rotational ladders are about an order of magnitude smaller than those within a rotational ladder. For the same reason, the vibrationally excited OH molecules radiatively decay preferentially into rotational states in the $^2\Pi_{3/2}$ ladder of the ground vibrational state. The OH molecules that decay to excited rotational states in the $^2\Pi_{3/2}$ ladder usually return to the ground rotational state by a sequence of radiative decays down the $^2\Pi_{3/2}$ ladder. If the transitions between the $^2\Pi_{3/2}, J = 5/2$ state and the $^2\Pi_{3/2}, J = 3/2$ state are optically thick, the return of population to the ground rotational state tends to invert the 1720 MHz transition.

A quantitative measure of the minimum OH column density, $(n_{\text{OH}} l)_{\min}$, required for the inversion of the 1612 MHz maser by NIR pumping is obtained by setting equal to unity the radial optical depth of the transition from the $v = 0, ^2\Pi_{3/2}, J = 3/2, F = 2$ level to the $v = 1, ^2\Pi_{1/2}, J = 1/2, F = 1$ level. This transition has the greatest line strength of any transition which links a level of the $v = 0, ^2\Pi_{3/2}, J = 3/2$ state with a level in the $^2\Pi_{1/2}$ ladder of the $v = 1$ state. This procedure yields

$$(n_{\text{OH}} l)_{\min} = 10^{15} \left(\frac{\mu_r}{\mu_{v-r}} \right)^2 \text{ cm}^{-2} \quad (21)$$

for an assumed line width of 1 km s^{-1} which is typical of the narrower maser lines from OH-IR stars. The quantity μ_r/μ_{v-r} is the ratio of the static dipole moment of the OH molecule in the $v = 0$ state to the dipole moment for transitions between the $v = 0$ and $v = 1$ states. The best determinations of $(\mu_r/\mu_{v-r})^2$ are from direct observations of the decay of vibrationally excited OH molecules in a flame which yield $(\mu_r/\mu_{v-r})^2 = 1.3 \times 10^4$ (Potter, Coltharp, and Worley 1971) and from quantitative measurements of vibration-rotation line intensities under controlled conditions which yield $(\mu_r/\mu_{v-r})^2 = 3.1 \times 10^3$ (d'Incan, Effantin, and Roux 1971). Both of these methods for determining $(\mu_r/\mu_{v-r})^2$ seem superior to the older method which relies on the small difference between the measured values of the static dipole moments for the $v = 0$ and $v = 1$ states and yields the much smaller value of $(\mu_r/\mu_{v-r})^2 = 1.1 \times 10^2$ (Phelps and Dalby 1965). Thus the best current data imply that NIR pumping of the 1612 MHz transition requires $(n_{\text{OH}} l)_{\min} > 10^{18} \text{ cm}^{-2}$ and probably $(n_{\text{OH}} l)_{\min} \approx 10^{19} \text{ cm}^{-2}$.

At OH column densities of order 10^{17} cm^{-2} or

smaller, the optical depths of the vibration-rotational lines are so low (even with the most optimistic value for the vibration-rotational transition moment) that the absorption of 2.8μ photons has a negligible effect on the population flow among the OH energy levels. Thus, if the OH column densities predicted from the calculation in Paper I are correct, the 1612 MHz masers must be pumped by FIR rather than NIR photons.

The relative magnitudes of the intensity variations of the maser emission and the infrared emission from OH-IR sources are more compatible with FIR than with NIR pumping. The ratio of the maximum to the minimum flux, F_{\max}/F_{\min} , is generally considerably greater at 2.8μ than at 1612 MHz (Harvey *et al.* 1974). For IRC +10011, F_{\max}/F_{\min} equals 7.0 at $\lambda = 2.2 \mu$, 4.4 at $\lambda = 3.5 \mu$, and 2.8 at 1612 MHz. Since the 1612 MHz masers appear to be saturated, one might expect the maser flux to vary in direct proportion to the flux in the pump lines. The fact that F_{\max}/F_{\min} is about twice as large at $\lambda = 2.8 \mu$ as it is at 1612 MHz must be considered as substantial, but not quite conclusive, evidence against NIR pumping. The FIR pump is powered by 35μ photons which are emitted by dust grains. It is difficult to accurately determine how the pump rate varies with the luminosity variations of the central star (cf. the discussion in § Vc). The dust grain temperature varies in response to the luminosity variations of the central star. The variations in T_d produce variations in the rate of emission of 35μ photons. The variations in pump rate and stellar luminosity are approximately related by equations (12) and (14). As an example, consider IRC +10011 whose total luminosity varies by a factor ~ 3.5 (Becklin 1974, private communication). Suppose that its minimum and maximum luminosity is $5.3 \times 10^3 L_\odot$ and $1.4 \times 10^4 L_\odot$, respectively. Then T_d at $r = 3 \times 10^{16} \text{ cm}$ varies between 110 K and 142 K. Corresponding to this temperature variation, the rate of emission of 35μ photons varies by a factor of 2.4. This value is in reasonable agreement, by a factor of 2.8, with the observed variation of the total 1612 MHz emission from IRC +10011.

e) Speculations

The evolutionary stage of the OH-IR stars is a fascinating topic for speculation. The mass loss rates, $\sim 3 \times 10^{-5} M_\odot \text{ yr}^{-1}$, suggest that the 1612 MHz OH-IR stars may be the precursors of planetary nebulae. It is possible that as more OH-IR sources are discovered, some of the central stars will be seen in a later phase of evolution where the hot stellar core is beginning to be exposed. When large numbers of OH-IR stars are known, it will be interesting to compare their space distribution with that of the planetaries.

We are indebted to an anonymous referee for helpful comments and criticisms. This research has been supported by NSF grant 4 MPS 7205045 A2 and MPS 73-04677-A01, and Office of Naval Research N 00014-67-A-0094.

REFERENCES

- Becklin, E. E. 1974, private communication.
- Castor, J. I. 1970, *M.N.R.A.S.*, **149**, 111.
- d'Incan, J., Effantin, C., and Roux, F. 1971, *J. Quant. Spectrosc. Rad. Transf.*, **11**, 1215.
- Goldreich, P., and Scoville, N. 1975, to be published (Paper I).
- Harvey, P. M., Bechis, K. T., Wilson, W. J., and Ball, J. A. 1974, *Ap. J. Suppl.*, No. 248, **27**, 331.
- Hyland, A. R., Becklin, E. E., Frogel, J. A., and Neugebauer, G. 1972, *Astr. and Ap.*, **16**, 204.
- Kwok, S., Gilman, R. C., and Woolf, N. J. 1974, preprint.
- Litvak, M. M. 1969, *Ap. J.*, **156**, 471.
- Litvak, M. M., and Dickenson, D. F. 1972, *Ap. J. Letters*, **12**, 113.
- Lucy, L. B. 1971, *Ap. J.*, **163**, 95.
- Masheder, M. R. E., Booth, R. S., and Davies, R. D. 1974, *M.N.R.A.S.*, **166**, 561.
- Phelps, D. H., and Dalby, F. W. 1965, *Canadian J. Phys.*, **43**, 144.
- Potter, A. E., Coltharp, R. N., and Worley, R. D. 1971, *J. Chem. Phys.*, **54**, 992.
- Reid, M. J. 1975, *Ap. J.*, to be published.
- Reid, M. J., and Muhleman, D. O. 1975, *Ap. J. (Letters)*, **196**, L35.
- Shklovsky, I. S. 1966, *Astr. Tsirk.*, No. 372.
- Sobolev, V. V. 1960, *Moving Envelopes of Stars* (Cambridge: Harvard University Press).
- Wilson, W. J., and Barrett, A. H. 1972, *Astr. and Ap.*, **17**, 385.
- Woolf, N. J. 1972, *Mém. Soc. Roy. Sci. Liège*, Series 6, **3**, 209.
- Zappala, R. R., Becklin, E. E., Matthews, K., and Neugebauer, G. 1974, *Ap. J.*, **192**, 109.

MOSHE ELITZUR: Weizmann Institute of Science, Rehovot, Israel

PETER GOLDREICH: Division of Geological and Planetary Sciences, California Institute of Technology, Pasadena, CA 91125

NICK SCOVILLE: Astronomy Department, University of Massachusetts, Amherst, MA 01002